2026 IEEE International Conference on Robotics and Automation (ICRA 2026)
June 1-5, 2026. Vienna, Austria

Selective Actuation for Microrobots based on Distributed Magnetic Field Design

Kaiwen Fang[1,2,†], Zhen Yang[1,2,†], Lianshuo Wang[3], Yuezhen Liu[1,2], Hui Chen[1,2], Yu Liu[1,2], and Jiangfan Yu[1,2]

***Abstract*— Mechanical stimulation is essential for regulating cellular processes such as proliferation, differentiation, and apoptosis. Magnetic microrobot swarms offer a promising platform for delivering targeted mechanical stimulation to cells via remote actuation under rotating magnetic fields. However, magnetic fields globally activate swarms in non-target regions, risking undesired biological effects. To overcome this limitation, we propose a spatially selective magnetic actuation strategy that confines mechanical stimulation to user-defined regions. A dual-robotic-arm magnetic actuation system is developed to generate a selective rotating magnetic field. The field ensures swarms have smooth rotation and longer chain formation within the target area, enabling effective mechanical stimulation, while swarms outside exhibit shortened chains and disordered motion. We further demonstrate that the area swept by the rotating chain of microrobots peaks within the targeted region but drops sharply beyond it. This approach provides a foundation for precise mechanostimulation in biomedical applications with minimal off-target effects.**

I. Introduction

Mechanical stimulation, such as stretch, pressure, or shear stress, plays a crucial role in triggering cellular biological processes through mechanotransduction [1], [2]. This process converts physical forces into biochemical signals, modulating ion channels [3], [4], regulating gene expression [5], and inducing cytoskeletal remodeling [6], thereby influencing cell proliferation, differentiation, migration, and other functions.

Magnetic microrobotic swarms, composed of millions of magnetic nanoparticles [7], [8], [9], [10], represent a promising technology for many biomedical applications [11], [12], [13], [14], [15]. Their miniature scale and capacity for remote manipulation via external magnetic fields enable them to mechanically stimulate cells with high precision [16], [17]. It has been reported that microrobot swarms, when actuated by a rotating magnetic field (RMF), can mechanically stimulate cells and regulate their biological processes through their collective motion. For example, the controlled rotation of the swarm can be directed to induce apoptosis in cancer cells by delivering precise mechanical forces to disrupt lysosomes, as demonstrated both in vitro and in vivo [18], [19]. Moreover, this same rotational motion generates sufficient shear stress to activate mechanosensitive ion channels on cell membranes, which in turn trigger downstream signaling cascades that regulate gene expression and cell differentiation [20], [21]. However, magnetic fields are applied globally, which means that microrobot swarms in non-targeted regions are also actuated, potentially triggering unintended mechanical stimulation of non-targeted cells and leading to undesired tissue outcomes [22]. Therefore, it is essential to develop a spatially selective magnetic actuation method, which can confine mechanical stimulation to targeted areas and ensure the safe application.

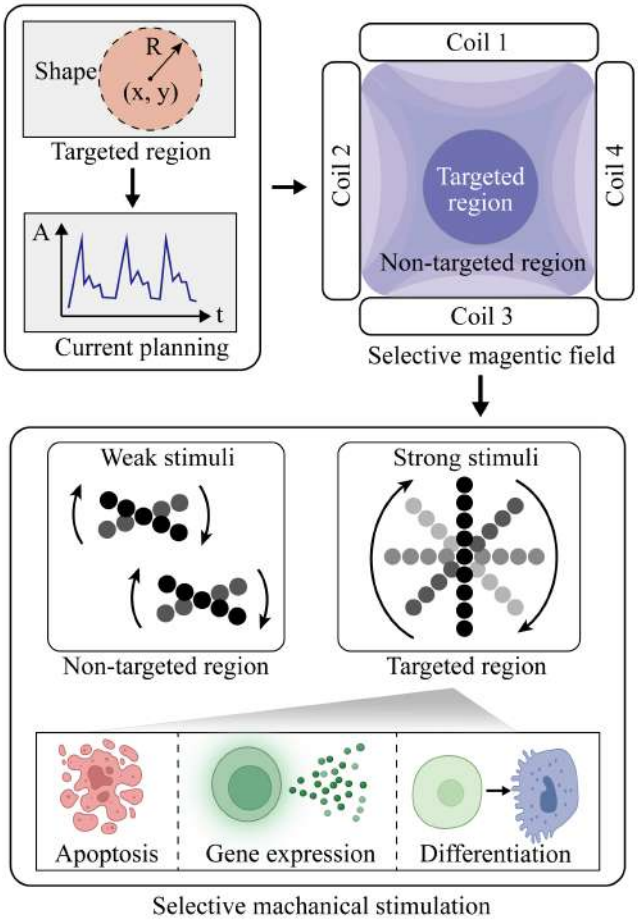

Figure 1. Schematic workflow of selective rotating magnetic fields for targeted mechanical stimulation.

Herein, to address this limitation, we propose a strategy for selective magnetic actuation that enables targeted cellular

This work was financially supported by the National Key R&D Program of China under Project No.2022YFA1207100, the Shenzhen Science and Technology Program under Projects No. JCYJ20241202124015021 and JCYJ20250604141050027.
(†Kaiwen Fang and Zhen Yang contributed equally to this work.) (Corresponding author: Jiangfan Yu, email: yujiangfan@cuhk.edu.cn).
[1]School of Science and Engineering, The Chinese University of Hong Kong, Shenzhen 518172, China.
[2]Shenzhen Institute of Artificial Intelligence and Robotics for Society (AIRS), Shenzhen 518129, China.
[3]Beihang University, Beijing 100191, China.

stimulation, as shown in Fig. 1. The behavior of microrobot swarms under rotating magnetic fields is investigated to offer empirical guidelines for the actuation strategy. Results reveal that the swarm chain length is highly dependent on magnetic field strength and frequency. Based on these findings, a selective rotating magnetic field is designed and generated by a dual robotic arm magnetic actuation system. An optimization algorithm determines the current sequences for each coil to produce a magnetic field that exceeds a critical strength threshold and maintains smooth rotation within a user-defined target region. Under such a magnetic field, microrobots inside the target region form longer chains and rotate smoothly, thereby producing effective mechanical stimulation. In contrast, swarms outside the target area experience shorter chain formations and irregular rotation. We further characterized the effective swept area of the rotating chains and found that it is significantly larger within the target zone and decreases rapidly with increasing distance from the center. These results confirm that the selective magnetic field enables spatially confined actuation of microrobotic swarms, paving the way for precise mechanical stimulation in biomedical applications.

II. Behaviors of Microrobot Swarms Under Rotating Magnetic Fields

Under a rotating magnetic field, microrobot swarms exhibit alignment of magnetic moments with the external field, resulting in interparticle attractive forces. These forces promote the self-assembly of the swarm into chain-like structures that rotate with the magnetic field.

When a particle chain in a low Reynolds number environment is subject to a magnetic field B and rotates at an angular speed ω, the stability of this chain is characterized by a modified Mason number [23], [24], denoted as R_T, which is defined as follows:

$$R_T = 64\frac{\mu_0 \eta \omega}{\chi_p^2 B^2}\frac{N^2}{(ln(N)+\frac{1.2}{N})} \quad (1)$$

where N is the number of particles in the chain, μ_0 is the permeability of free space, χ_p is the effective magnetic susceptibility of the nanoparticles, and η is the dynamic viscosity of the fluid. If $R_T < 1$, the magnetic torque dominates over the viscous drag torque, and the chain remains stable. When $R_T = 1$, the magnetic and viscous torques are balanced, and the chain rotates synchronously with the magnetic field but is on the verge of fragmentation. If $R_T > 1$, the viscous torque exceeds the magnetic binding torque, leading to the breakup of the chain.

To study how magnetic field parameters govern the self-assembly of microrobotic swarms into chain structures, the chain length is characterized under rotating magnetic fields with different strengths and frequencies, as shown in Fig. 2. A microrobot swarm suspends in a tank filled with polyvinylpyrrolidone (PVP) solution. The viscosity of the PVP solution is set to 20 cP to closely mimic the physical conditions of a cell-culture environment.

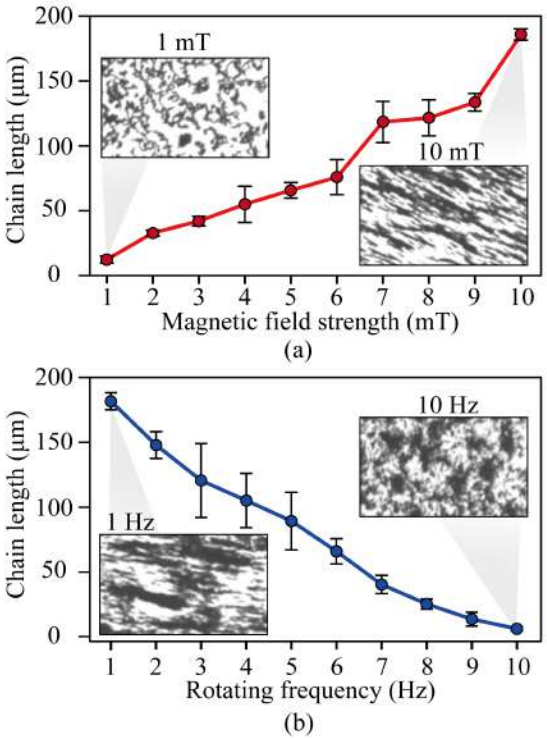

Figure 2. Characterization of chain length under different rotating magnetic field parameters. (a) The relationship between chain length and magnetic field strength. The magnetic field frequency is 0.5 Hz. (b) The relationship between chain length and magnetic field frequency. The magnetic field strength is 10 mT.

The relationship between chain length and field strength is illustrated in Fig. 2(a). The chain length increases with the magnetic field strength. At a low field strength of 1 mT, the swarm remains dispersed, forming only small clusters on the substrate, as shown in the inset. In contrast, increasing the field strength to 10 mT induces the formation of distinct chain structures, with an average chain length reaching 185.9 μm. This phenomenon arises because higher field strengths induce larger magnetic dipole moments within the particles, enhancing the attractive dipole-dipole interactions between them. Consequently, particles align end-to-end, leading to significantly longer chains as the magnetic field intensifies.

The influence of rotational frequency on chain length is also investigated, as presented in Fig. 2(b). Here, an inverse relationship is observed. The chain length decreases significantly with increasing rotating magnetic field frequency. This phenomenon occurs because faster rotation subjects the particle chains to greater viscous drag forces from the surrounding fluid. The increased hydrodynamic forces disrupt the stability of the chain structure, causing chains to fragment. As a result, at higher frequencies, the swarm transitions from organized chains to rotating, unconsolidated clusters, and distinct chain-like structures are no longer sustained.

III. Experimental Setup

Figure 3 shows the dual-robotic-arm magnetic actuation system designed to generate a selective magnetic field for microrobot swarm control. Each robotic arm integrates two

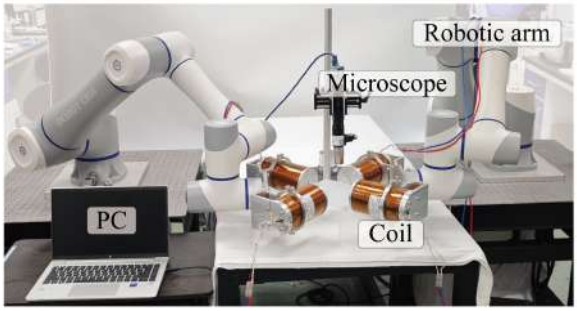

Figure 3. Dual-robotic-arm magnetic actuation system.

electromagnetic coils at its end-effector. By coordinating the movement of the robotic arms, a selective magnetic field can be generated at any point within the expansive workspace. To observe the resulting swarm behavior, a solution containing magnetic nanoparticles is introduced into a tank filled with PVP solution, and a microscope positioned directly above the tank provides real-time, high-resolution monitoring of the microrobot dynamics under the applied magnetic fields.

IV. MAGNETIC FIELD DESIGN

A. Magnetic field design consideration

The magnetic swarm behavior reveals a critical dependence of chain length on both the applied magnetic field strength and its rotational frequency. Specifically, a critical field strength is required to form and sustain chains beyond a certain length. If the field strength drops below this threshold, the collective structure cannot maintain its integrity, leading to discontinuous actuation.

An assumption can be further proposed that fluctuations in field strength can lead to inconsistent actuation behavior. Under a rotating magnetic field, if the field strength varies within a cycle, chains that formed during high-strength periods may fail to rotate in low-strength intervals. This introduces a phase lag between the chain direction and the field direction, and when the field strength increases again, the chain may undergo a sudden rotational jump to realign the field direction. The angular speed spike ultimately causes chain fragmentation and prevents the formation of long, coherent structures. Therefore, to achieve selective swarm stimulation, it is essential to maintain a field strength above the critical level while ensuring smooth and consistent rotation in the targeted region.

B. Actuation strategy and magnetic field design

As illustrated in Fig. 1 and 3, the magnetic actuation system consists of four coils, each oriented perpendicularly to its adjacent counterparts. To generate the required non-uniform rotating magnetic field while confining actuation to targeted regions, current sequences adhere to four fundamental principles:

1. In a rotating magnetic field, the currents in the electromagnetic coils alternate sequentially, resulting in stronger magnetic fluctuations in regions closer to the individual coils. To ensure stable and consistent magnetic field strength during operation, the targeted region should be positioned near the center of four coils, where field uniformity is ensured.

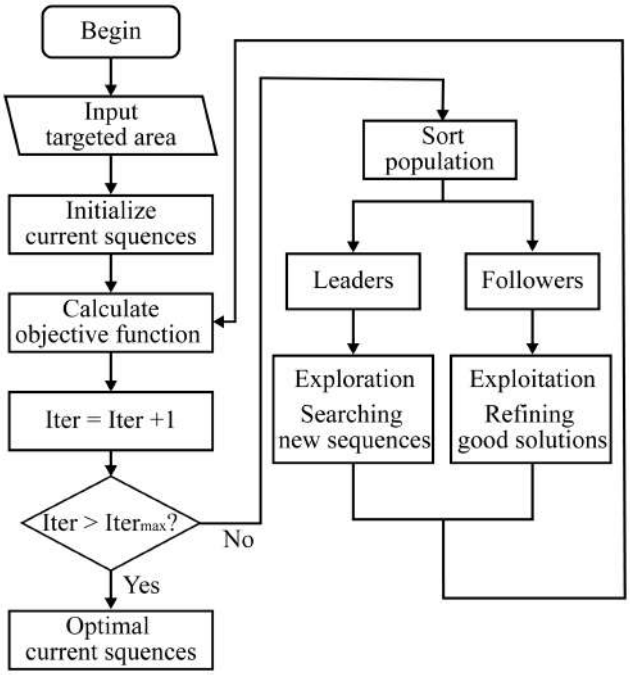

Figure 4. Flow chart of the swarm intelligence algorithm for searching optimal current sequences.

2. To generate a nonuniform rotating magnetic field, for the k-th quarter cycle T_k (k=1,2,3,4), the current in coil j is given by:

$$I_j(t) = A_j(t) \cdot \sin\left(\omega t + \varphi_j + \frac{k\pi}{2}\right), t \in T_k \tag{2}$$

where $A_j(t)$ denotes the time-varying current amplitude, ω is the angular frequency, and $\varphi_j \in \{0, 0.5\,\pi, \pi, 1.5\,\pi\}$, which corresponds to the physical orientation of coil j.

3. The magnetic field strength must exceed a critical threshold $B_{critical}$ throughout the entire targeted region Q over the cycle:

$$B\left(t, p, \left\{I_j(t)\right\}_{j=1}^{4}\right) \geq B_{critical}, \forall p \in Q, t \in T \tag{3}$$

4. To minimize unintended field exposure in non-target regions U, the current amplitudes should be optimized to maximize the area where the field remains below $B_{critical}$. This is formulated as the following optimization problem:

$$A^* = \arg\max_{A} \Sigma_{\{t \in T\}} \Sigma_{\{p \in U\}} \Sigma_{j=1}^{4} \mathrm{I}\left\{B\left(t, p, I_j(t)\right) < B_{critical}\right\} \tag{4}$$

C. Current planning algorithm for magnetic field generation

Given the high complexity of the potential current sequences, the corresponding solution space becomes exceedingly large. To efficiently identify optimal current amplitudes that meet the specified requirement, an improved swarm intelligence algorithm is employed.

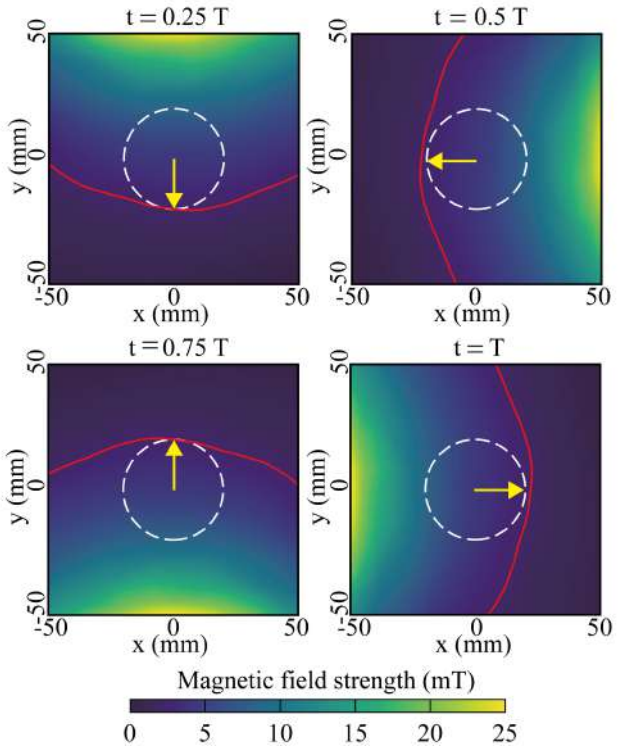

Figure 5. Spatial distribution of the simulated magnetic field at each quarter. The red lines represent the fields where the strengths are equal to the critical magnetic field strength. The white dotted lines represent the targeted region. In this case, the critical magnetic field strength is 5 mT, and the radius of the targeted region is 20 mm.

As shown in Fig. 4, the algorithm operates on the principles of population-based metaheuristics. Initially, a population of candidate particles is generated, each representing a unique set of current parameters $\{A_1(t), A_2(t), A_3(t), A_4(t)\}$ applied across the four coils. Throughout the iterative process, each particle adjusts its position based on a combination of individual and collective learning:

1. Individual learning: each particle tends to move towards its own historically best solution.

2. Social learning: particles are simultaneously attracted to the globally best solution found so far.

The iterative update rule can be expressed in a general form:

$$S_i^{m+1} = S_i^m + \alpha \cdot r_1 \left(S_{best_i} - S_i^m \right) + \beta \cdot r_2 \left(S_{global} - S_i^m \right) \quad (5)$$

where S_i^m denotes the solution of particle i at iteration m, S_{best_i} its personal best, S_{global} is the global best solution, and r_1 , r_2 are uniformly distributed random numbers. The coefficients α and β control the balance between exploration and exploitation. At each iteration, the updated candidate solutions are evaluated against the constraints in Eq. (2) and (3), and the objective function in Eq. (4). Solutions that violate the constraints are penalized, effectively steering the swarm toward both feasible and optimal regions of the solution space.

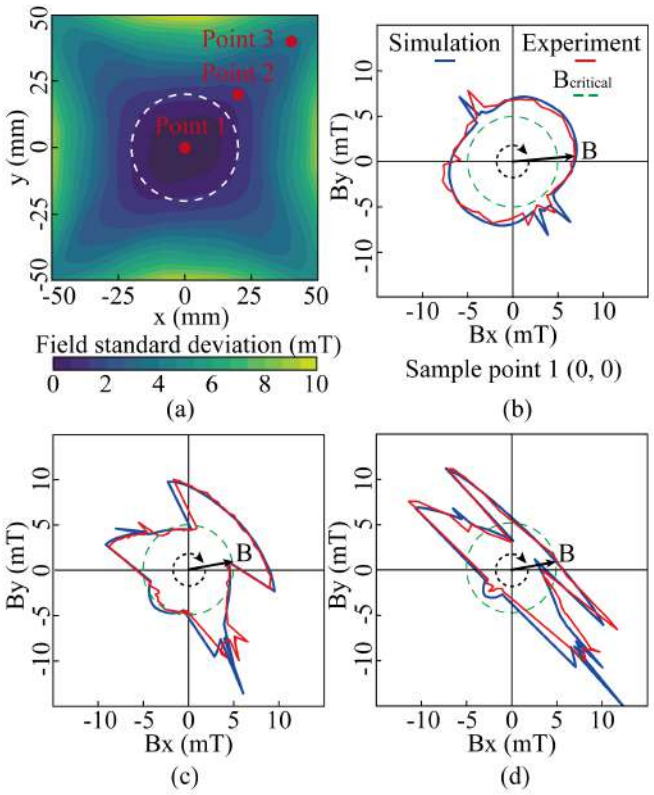

Figure 6. Spatial mapping of field fluctuations and magnetic fields at sampling points. (a) Standard deviation of the selective rotating magnetic field. (b) Trajectory of the magnetic field vector at (0,0). (c) Trajectory of the magnetic field vector at (20,20). (d) Trajectory of the magnetic field vector at (40,40).

V. Magnetic Field Simulation and Validation

Here, the critical magnetic field strength $B_{critical}$ is set to 5 mT, and the targeted region is defined as a circular area with a radius of 20 mm. Figure 5 illustrates the transient magnetic field distribution at each quarter of a cycle. The contour corresponding to $B_{critical}$ consistently encloses the outer edge of the target zone across all the cycle. It indicates that the magnetic field strength remains above the critical threshold throughout the entire target region at each phase of actuation.

To characterize the fluctuation of the magnetic field strength, the standard deviation of the field strength across the cycle is studied, as shown in Fig. 6(a). Results show the standard deviation remains below 2 mT within the targeted region, indicating highly consistent field strength over time. Beyond the targeted region, the standard deviation increases rapidly with radial distance, revealing a rapid decline in field stability outside the target boundary.

To further study the magnetic field pattern, we characterize the magnetic field vector in a cycle at three sample points. As shown in Fig. 6(a), three points are taken at (0,0), (20,20) and (40,40). The trajectories of the field vector at these points are presented in Fig. 6(b), (c), and (d), respectively. The magnetic field vector at the center (point 1) traces a continuous, near-circular path and maintains a field strength consistently above

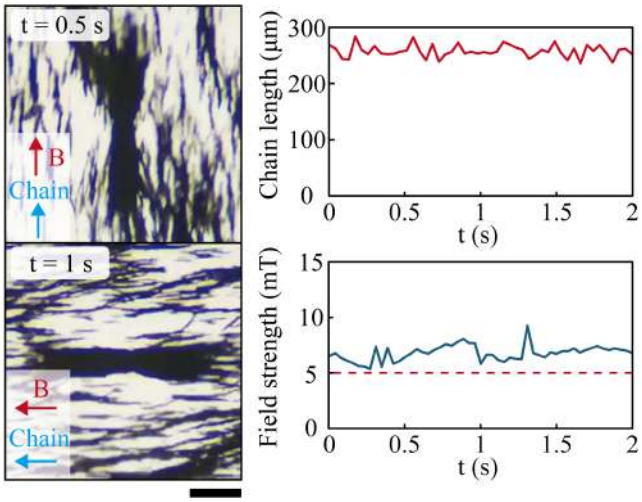

Figure 7. Swarm behavior and the corresponding magnetic field strength in the targeted region (point 1). The red dotted line represents the critical field strength. Scale bar, 50 μm.

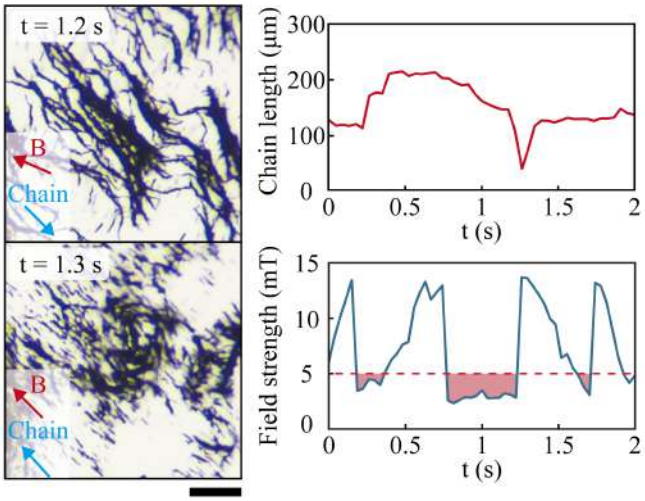

Figure 9. Swarm behavior and the corresponding magnetic field strength in the non-targeted region (point 3). The red dotted line represents the critical field strength. The light pink region represents the period during which the magnetic field strength is below the critical field strength. Scale bar, 50 μm.

the critical threshold of 5 mT. At point 3, the trajectory becomes markedly irregular, and the magnitude frequently drops below the critical value.

VI. Experimental Results

To validate the effectiveness of the spatially selective magnetic field in actuating microrobot swarms for targeted mechanical stimulation, we compare the behavior of swarms located at two distinct points: point 1 (within the target center) and point 3 (outside the target region). As shown in Fig. 7, due to the stable field strength that remains above the critical threshold, the swarm at point 1 exhibits stable and continuous rotation synchronously with the magnetic field direction. Throughout the cycle, the average chain length remains stable within a range of 236.3 to 283.8 μm, confirming that the magnetic conditions are sufficient to sustain collective integrity and smooth motion. In contrast, the swarm at point

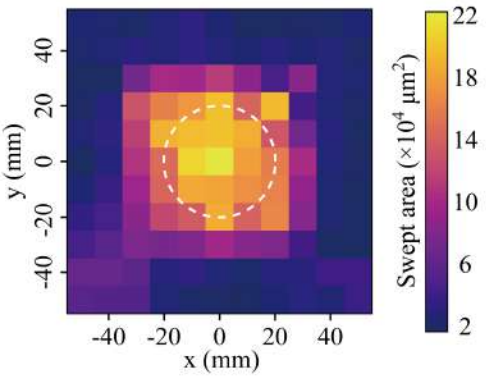

Figure 8. Swept area of the particle chains. The white dotted line represents the edge of the targeted region.

3 demonstrates markedly different behavior, as presented in Fig. 8. At this point, the magnetic field strength periodically falls below the critical value. A significant phase lag occurs between the particle chains and the applied magnetic field at 1.2 s. It is because the magnetic field strength drops below the critical value, rendering it insufficient to drive the preformed chain structures. When the field strength abruptly increases at t = 1.3 s, the swarm undergoes a sudden large-angle rotation in an attempt to realign with the field direction. The rapid motion results in a high angular acceleration, ultimately leading to chain disassembly.

To further evaluate the effectiveness of selective mechanical stimulation across the workspace of the magnetic field, we characterize the swept area of the particle chains, which directly reflects the spatial extent of mechanical stimulation exerted by the swarm. As shown in Fig. 9, the swept area reaches its maximum within the targeted region and decreases sharply with increasing distance from the center. This sharp change in the swept area demonstrates that the capability of the magnetic field to selectively control the microrobot swarm's action, proving the actuation strategy can effectively confine the mechanical stimulation to a targeted region.

VII. Conclusion

In this study, we develop a strategy for spatially selective actuation of magnetic microrobot swarms to achieve targeted mechanical stimulation. The microrobot swarm behavior under rotating magnetic fields is investigated. The magnetic fields enable microrobotic swarms to self-assemble into chain-like structures, with field strength and frequency playing crucial roles in determining chain length and stability. Higher magnetic field strength promotes longer chain formation by strengthening magnetic attraction between particles, while increased rotational frequency leads to chain fragmentation due to greater fluid resistance.

Based on the findings above, a selective actuation strategy is designed, which is supported by an optimization algorithm that significantly accelerates the search for optimal current sequences. The generated magnetic field maintains a field

strength above the critical threshold within a user-defined target region. Inside the targeted region, the field remains uniform, whereas outside, the field exhibits substantial fluctuations, which means it often drops below the critical threshold. Both simulation and experimental results demonstrate excellent agreement, validating the precision of the proposed magnetic control approach. A dual robotic-arm magnetic actuation system is designed, which ensures the selective rotating magnetic field can be generated at any point within the workspace.

We finally validate that the spatially selective magnetic field enables selective microrobot stimulation inside a targeted region. Within the targeted region, the swarm exhibits stable rotation and consistent chain morphology. In contrast, outside the target region, fluctuation of field strength disrupts synchronization, causing phase lag and abrupt swarm rotation that ultimately fragments the chains. The swept area of the chains, directly linked to mechanical stimulation, is maximized inside the target and declines sharply with distance from the center. These results demonstrate the high spatial resolution and effectiveness of our actuation strategy in confining mechanical microrobot stimulation to a predefined region.

Our future work will focus on improving the precision of the magnetic field and achieving more distinct behavioral transitions of the microrobot swarm at the boundaries of the target region. The strategy will be validated in biologically relevant environments such as animal models, to assess its efficacy and robustness under clinically representative conditions. We hope these steps will strengthen the translational potential of the proposed method for applications in targeted therapy.

REFERENCES

[1] J. An *et al.*, "Mechanical stimuli-driven cancer therapeutics," *Chem. Soc. Rev.*, vol. 52, no. 1, pp. 30–46, 2023.

[2] Y. Artemenko, L. Axiotakis, J. Borleis, P. A. Iglesias, and P. N. Devreotes, "Chemical and mechanical stimuli act on common signal transduction and cytoskeletal networks," *Proc. Natl. Acad. Sci. U.S.A.*, vol. 113, no. 47, Nov. 2016.

[3] S. A. Gudipaty *et al.*, "Mechanical stretch triggers rapid epithelial cell division through Piezo1," *Nature*, vol. 543, no. 7643, pp. 118–121, Mar. 2017.

[4] Z.-H. Wang *et al.*, "Mechanical stimulation from the surrounding tissue activates mitochondrial energy metabolism in *Drosophila* differentiating germ cells," *Developmental Cell*, vol. 58, no. 21, pp. 2249-2260.e9, Nov. 2023.

[5] X. Di *et al.*, "Cellular mechanotransduction in health and diseases: from molecular mechanism to therapeutic targets," *Sig Transduct Target Ther*, vol. 8, no. 1, p. 282, July 2023.

[6] C. M. Bidan *et al.*, "Magneto-active substrates for local mechanical stimulation of living cells," *Sci Rep*, vol. 8, no. 1, p. 1464, Jan. 2018.

[7] J. Yu, T. Xu, Z. Lu, C. I. Vong, and L. Zhang, "On-Demand Disassembly of Paramagnetic Nanoparticle Chains for Microrobotic Cargo Delivery," *IEEE Trans. Robot.*, vol. 33, no. 5, pp. 1213–1225, Oct. 2017.

[8] J. Yu, L. Yang, and L. Zhang, "Pattern generation and motion control of a vortex-like paramagnetic nanoparticle swarm," *The International Journal of Robotics Research*, vol. 37, no. 8, pp. 912–930, July 2018.

[9] J. Yu, L. Yang, X. Du, H. Chen, T. Xu, and L. Zhang, "Adaptive Pattern and Motion Control of Magnetic Microrobotic Swarms," *IEEE Transactions on Robotics*, vol. 38, no. 3, pp. 1552–1570, June 2022.

[10] Y. Liu, H. Chen, Q. Zou, X. Du, Y. Wang, and J. Yu, "Automatic Navigation of Microswarms for Dynamic Obstacle Avoidance," *IEEE Transactions on Robotics*, vol. 39, no. 4, pp. 2770–2785, Aug. 2023.

[11] S. A. Abbasi *et al.*, "Autonomous 3D positional control of a magnetic microrobot using reinforcement learning," *Nat Mach Intell*, vol. 6, no. 1, pp. 92–105, Jan. 2024.

[12] J. Law *et al.*, "Microrobotic swarms for selective embolization," *Sci. Adv.*, vol. 8, no. 29, p. eabm5752, July 2022.

[13] H. Chen *et al.*, "Active microgel particle swarms for intrabronchial targeted delivery," *Sci. Adv.*, vol. 11, no. 11, p. eadr3356, Mar. 2025.

[14] X. Du *et al.*, "Active exploration and reconstruction of vascular networks using microrobot swarms," *Nat Mach Intell*, vol. 7, no. 4, pp. 553–564, Mar. 2025.

[15] Q. Wang *et al.*, "Tracking and navigation of a microswarm under laser speckle contrast imaging for targeted delivery," *Sci. Robot.*, vol. 9, no. 87, p. eadh1978, Feb. 2024.

[16] L. Yang, Y. Zhang, Q. Wang, K.-F. Chan, and L. Zhang, "Automated Control of Magnetic Spore-Based Microrobot Using Fluorescence Imaging for Targeted Delivery With Cellular Resolution," *IEEE Transactions on Automation Science and Engineering*, vol. 17, no. 1, pp. 490–501, Jan. 2020.

[17] W. Dou *et al.*, "Robotic manipulation of cardiomyocytes to identify gap junction modifiers for arrhythmogenic cardiomyopathy," *Sci. Robot.*, vol. 9, no. 95, p. eadm8233, Oct. 2024.

[18] Y. Shen *et al.*, "Adaptive Control of Nanomotor Swarms for Magnetic-Field-Programmed Cancer Cell Destruction," *ACS Nano*, vol. 15, no. 12, pp. 20020–20031, Dec. 2021.

[19] X. Wang *et al.*, "Mechanical nanosurgery of chemoresistant glioblastoma using magnetically controlled carbon nanotubes," *Sci. Adv.*, vol. 9, no. 13, p. eade5321, Mar. 2023.

[20] X. Wang *et al.*, "Magnetic Measurement and Stimulation of Cellular and Intracellular Structures," *ACS Nano*, vol. 14, no. 4, pp. 3805–3821, Apr. 2020.

[21] A. Hillion *et al.*, "Real-Time Observation and Analysis of Magnetomechanical Actuation of Magnetic Nanoparticles in Cells," *Nano Lett.*, vol. 22, no. 5, pp. 1986–1991, Mar. 2022.

[22] T. Gwisai, N. Mirkhani, M. G. Christiansen, T. T. Nguyen, V. Ling, and S. Schuerle, "Magnetic torque–driven living microrobots for increased tumor infiltration," *Sci. Robot.*, vol. 7, no. 71, p. eabo0665, Oct. 2022.

[23] A. Van Reenen, A. M. De Jong, J. M. J. Den Toonder, and M. W. J. Prins, "Integrated lab-on-chip biosensing systems based on magnetic particle actuation – a comprehensive review," *Lab Chip*, vol. 14, no. 12, pp. 1966–1986, 2014.

[24] J. Law, H. Chen, Y. Wang, J. Yu, and Y. Sun, "Gravity-resisting colloidal collectives," *Sci. Adv.*, vol. 8, no. 46, p. eade3161, Nov. 2022.